© 2020 IEEE. Personal use of this material is permitted. Permission from IEEE must be obtained for all other uses, in any current or future media, including reprinting/republishing this material for advertising or promotional purposes, creating new collective works, for resale or redistribution to servers or lists, or reuse of any copyrighted component of this work in other works.

Anti-Islanding Method for Houses Equipped with Electric Vehicles and Photovoltaic System

U.B. Irshad [1], S. Rafique[1], M.J. Hossain[2], S.C. Mukhopadhyay[1]
[1] School of Engineering, Macquarie University, Australia
[2] School of Electrical and Data Engineering,UTS, Australia
*usama.bin.irshad@gmail.com

***Abstract*—Integration of electric vehicles (EVs) are exponentially increasing in the global market and by enabling vehicle-to-grid (V2G) EVs can inject power back into the grid. However, in an event of unintentional islanding, injecting power into the grid may causes potential safety threats to people, equipment, and power system. This paper proposes an adaptive reactive power mismatch method to detect islanding events. When islanding occurs, the proposed method drifts the system frequency away from the nominal value. Then the islanding event is detected based on frequency variations. Results show that the proposed method effectively detects islanding event in all conditions and negligible non detection zone. Moreover, it can detect islanding within 0.801 milliseconds**

Keywords— Electric vehicle, Islanding detection method, Photovoltaic system.

Nomenclature

i_{dref}	Reference signal for i_d
i_{qref}	Reference signal for i_q
L	Inductance of L_{filter}
V_{td}	Terminal voltage
V_{sd}	d component of line voltage
ω_O	Angular frequency of the system
i_q	q component of line current
P_{sref}	Reference signal for active power
Q_{sref}	Reference signal for reactive power
R	Resistance
r_{on}	Filter resistance
Q_{ref}	New reference set for reactive power
V_{sq}	Q component of line voltage
i_d	d component of line current
u_d	Active power PI controller signal
f_O	Rated frequency of the system
K_p	Proportional gain of PI controller
K_i	Integral gain of PI controller
τ_i	Time constant
P_L	Active power consumed by Load
P_{DG}	Active power available in DG.
P_{grid}	Active power from grid.
Q_L	Reactive power consumed by Load
Q_{DG}	Reactive power available in DG.
Q_{grid}	Reactive power from grid.
V_{PCC}	Instantaneous value of voltage at PCC
ΔP	Active power from grid
V_L	Line-to-line voltage
Δf_o	Change in frequency
V_N	Nominal voltage of the system
f_{min}	Minimum allowable frequency
ΔQ	Change in reactive power
f_{max}	Maximum allowable frequency

I. INTRODUCTION

Due to environmental concerns, the adoption of electric vehicles (EVs) is beginning to increase in many countries. By enabling vehicle to grid (V2G) EVs can supply power to the grid or local load. For example, Tesla EV can supply power a house up to 5 days. The renewable energy resources (like photovoltaic (PV) system) are installed near to the local loads. Even, the rooftop photovoltaic system combined with EV can easily support the household load and inject additional power back into the grid (Fig. 1). In the event of a fault, the utility grid disconnects itself from the system and send line workers to fix the issue. But it might be possible that some house equipped with PV and EV are supplying power without knowing that the utility grid is disconnected. So, this active part (island) in the power system is dangerous to the line worker. Therefore, the house must detect the islanding event and disconnect the itself from the utility grid.

The islanding detection techniques can be classified as central (remote) and local methods. The central methods are communication-based. Power quality is not affected by central methods. However, the implementation of central methods is very costly at the consumer/household level. Local methods include passive, active methods. Among them over/under frequency protection (OFP/UFP) [1]–[3], over/under voltage protection (OVP/UVP) [4]–[8] and phase jump detection [5], [9] are extensively used passive methods. Passive methods determine islanding by sensing voltage and frequency at the point of common coupling (PCC). However, the passive method fails to detect islanding when DG is capable of meeting the local load demand. The active frequency drift (AFD) [10]–[13], slip mode frequency shift [14]–[18] and Sandia frequency shift (SFS) [19] are the commonly used active techniques for islanding detection. However, active methods fail when the penetration of DGs increases and power mismatch between load and DG is negligible. In [20], [21], phase-locked loop is used for islanding detection. However, it can only detect the islanding event when the load is reactive. To conclude, most method proposed in the literature have a large non-detection zone,

XXX-X-XXXX-XXXX-X/XX/$XX.00 ©20XX IEEE

long detection time, power quality issues and degrade the performance of the system. Therefore, an efficient islanding detection technique with ideally zero non-detection zone (NDZ) is needed.

Adaptive reactive power mismatch based on voltage variation is proposed to detect islanding. When islanding occurs, the proposed algorithm drifts the frequency away from its nominal value and disconnect the system.

II. System Discription

Fig. 1 shows the house equipped with PV system, EV and battery energy storage system (BESS). The PV, EV, BESS and utility grid are exchanging power between each other. The grid connected voltage source converter (VCS) is controlling the AC and DC power.

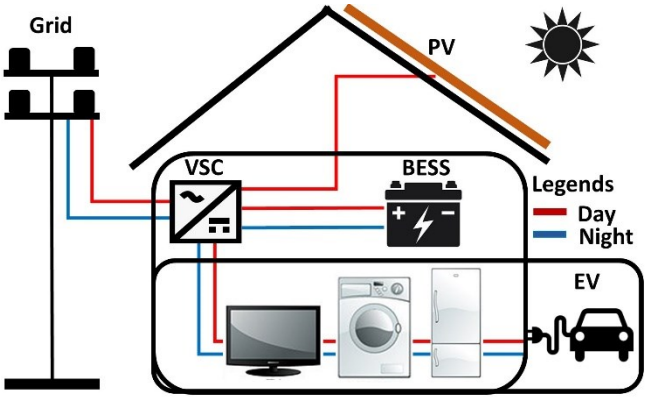

Fig. 1. *Household equipped with EV, PV and BESS*

The schematic diagram of grid-connected voltage source converter (VSC) is shown in Fig. 2. The resistance Z_T at AC side of VSC represents the conductance power loss. The DC side of VSC is considered as a constant DC voltage source. VSC is connected with AC system through series impedance $R + r_{on}$ and L filter. The L filter is tuned to reduce harmonics in the system. Z_g is the grid input impedance. Active and reactive powers are controlled by phase angle and line current amplitude of VSC with respect to point of common coupling (PCC) voltage.

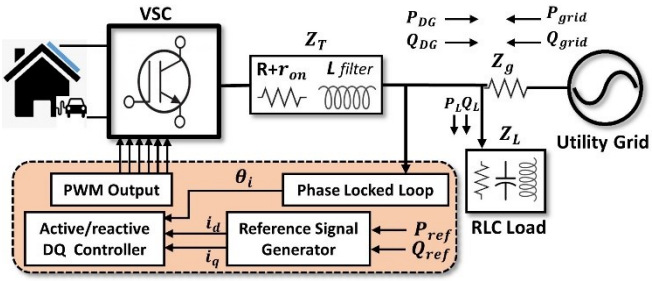

Fig. 2. *System description*

A. DQ-frame current controller

Fig. 3 illustrates the current controller in DQ-frame[22]. Real and reactive powers are controlled by i_d and i_q. Whereas the error signals are represented by e_d and e_q, Here, u_d and u_q denote the output of the PI controller. V_{DC} is dc voltage across the DC link capacitor. i_{dref} and i_{qref} are the active and reactive power reference and can be computed using (1)-(2).

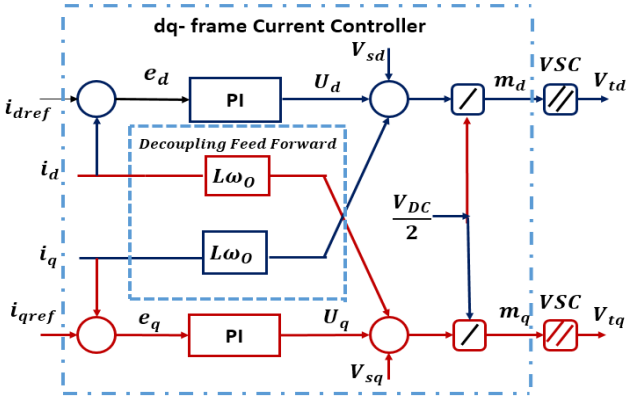

Fig. 3. *Dq-frame current controller*

$$i_{dref}(t) = \frac{2}{3V_{sd}} P_{sref}(t) \quad (1)$$

$$i_{qref}(t) = -\frac{2}{3*V_{sd}} Q_{sref}(t) \quad (2)$$

Equations (3)-(4) describe the dynamic model of the AC system. Here r_{on}=0.88 mΩ, R=0.75 mΩ, inductive reactance L is 80 mH and ω_O is the nominal frequency of 60 Hz.

$$L\frac{di_d}{dt} = V_{td} - V_{sd} + L\,\omega_O i_q - (R + r_{on})i_d \quad (3)$$

$$L\frac{di_q}{dt} = V_{tq} - V_{sq} - L\omega_O i_d - (R + r_{on})i_q \quad (4)$$

Here state variables are i_d and i_q, control inputs are V_{td} and V_{tq}. The disturbances in the system is represented by V_{sd} and V_{sq}. V_{td} and V_{tq} are described as

$$V_{td}(t) = u_d - Lf_O i_q + V_{sd} \quad (5)$$

$$V_{tq}(t) = u_q + Lf_O i_d + V_{sq} \quad (6)$$

The gain of the proportional-integral (PI) controller can be determined by using (7). Here τ_i is the time constant and its value depends on the system requirement. Value of τ_i can range from 0.5 to 5 milliseconds. In this work, the value of τ_i is 3 ms.

$$K_p = {}^{L}/_{\tau_i} \quad \text{and} \quad K_i = {}^{(R + r_{on})}/_{\tau_i} \quad (7)$$

B. Adaptive reactive power reference

Both grid and DG are delivering power to RLC load. Active and reactive powers consumed by the load can be computed as

$$P_L = P_{DG} + P_{grid} = 3V_{PCC}^2 \frac{1}{R} \quad (8)$$

$$Q_L = Q_{DG} + Q_{grid} = 3V_{PCC}^2 \left(\frac{1}{2\pi f_o L} - 2\pi f_o C\right) \quad (9)$$

Here f_o and V_{pcc} are the nominal frequency and voltage at PCC and L, R, C are inductive, resistive, and the capacitive component of the load. Active and reactive powers from the grid are denoted as P_{grid} and Q_{grid} respectively. After islanding, active power mismatch ΔP causes the voltage to deviate from its nominal value and reactive power mismatch

ΔQ variates the frequency of the system. ΔP *and* ΔQ can be computed by using (10)-(11) [23].

$$\Delta P = P_{DG}\left(\frac{1}{(1+\Delta V/V_{pcc})^2} - 1\right) \quad (10)$$

$$\Delta Q = \frac{3V_{PCC}^2}{2\pi f_o L}\left(1 - \frac{f_o^2}{(f_o+\Delta f_o)^2}\right) \quad (11)$$

It is observed that variation in frequency due to reactive power mismatch is more significant as compared to active power mismatch. Therefore, based on voltage variation, this work introduces adaptive reactive power mismatch. Equations (12) and (13) are used to update the reactive power references based on the change in voltage at PCC. If the voltage at PCC is greater than $1.01*V_N$, it means DG is suppling more active power than load consumption, so the reactive power reference is set by using (12).

$$Q_{ref1} = -|V_L|^2 * \left(\frac{f_o - f_{min}}{f_o}\right) + Q_L \quad (12)$$

Here V_L is the line to line voltage at PCC and f_{min} is the minimum allowable threshold value of frequency. Here its value is 59.4 Hz. If the voltage at PCC is less than $0.98\ V_N$, the Q_{ref} is change by using (13).

$$Q_{ref2} = -|V_L|^2 * \left(\frac{f_o - f_{max}}{f_o}\right) + Q_L \quad (13)$$

The maximum allowable frequency is shown by f_{max} . Here f_{max} is 60.5 Hz. Equations (12) and (13) update the reactive power reference and ensuring that the frequency will deviate when islanding occurs. It will help in detecting the islanding for a resistive load having a resonance frequency of f_o (i.e. 60 Hz)

$$Q_{ref} = \begin{cases} Q_{ref1} & V_{PCC} > 1.01V_N \\ Q_{ref2} & V_{PCC} < 0.98\ V_N \\ Q_L & 0.98V_N < V_{PCC} < 1.02V_N \end{cases} \quad (14)$$

Reference signal generator (RSG) is shown in Fig. 2. RSG generates reactive power reference by using (14).

III. RESULTS

This section presents the efficacy of the proposed islanding detection method. The parameters used in simulation are tabulated in Table 1. The controller is tested based on a simultaneous change in both active and reactive power reference. Fig. 4 (a) represents the three-phase voltage of the system. The controller tracks the reference point of active and reactive power by regulating the line current. Fig. 4 (b), shows the variations in current due to change in active and reactive power reference. Fig. 4 (c) shows the simultaneous change in reference of active power. Active power reference changes from zero to 200 W at the beginning and at 0.3 seconds, reference power changes from 200 to 400 W. Fig. 4 (d) shows that at the beginning reactive power varies from zero to 50 VAR and at 0.1 seconds it varies from 50 to -100 VAR. In Fig. 4 (c) and Fig. 4 (d), active and reactive

Table 1. MATLAB Simulation Parameters

Parameters	Values
Z_{L1} (RC)	5 Ω // 50 µF
Z_{L2} (RL)	5 Ω // 70 mH
Z_{L3} (RLC)	5 // 300 µF // 23.3 mH
Z_g	100 Ω
V_g	230 V
$f_{nominal}$	60 Hz
f_s	20 KHz

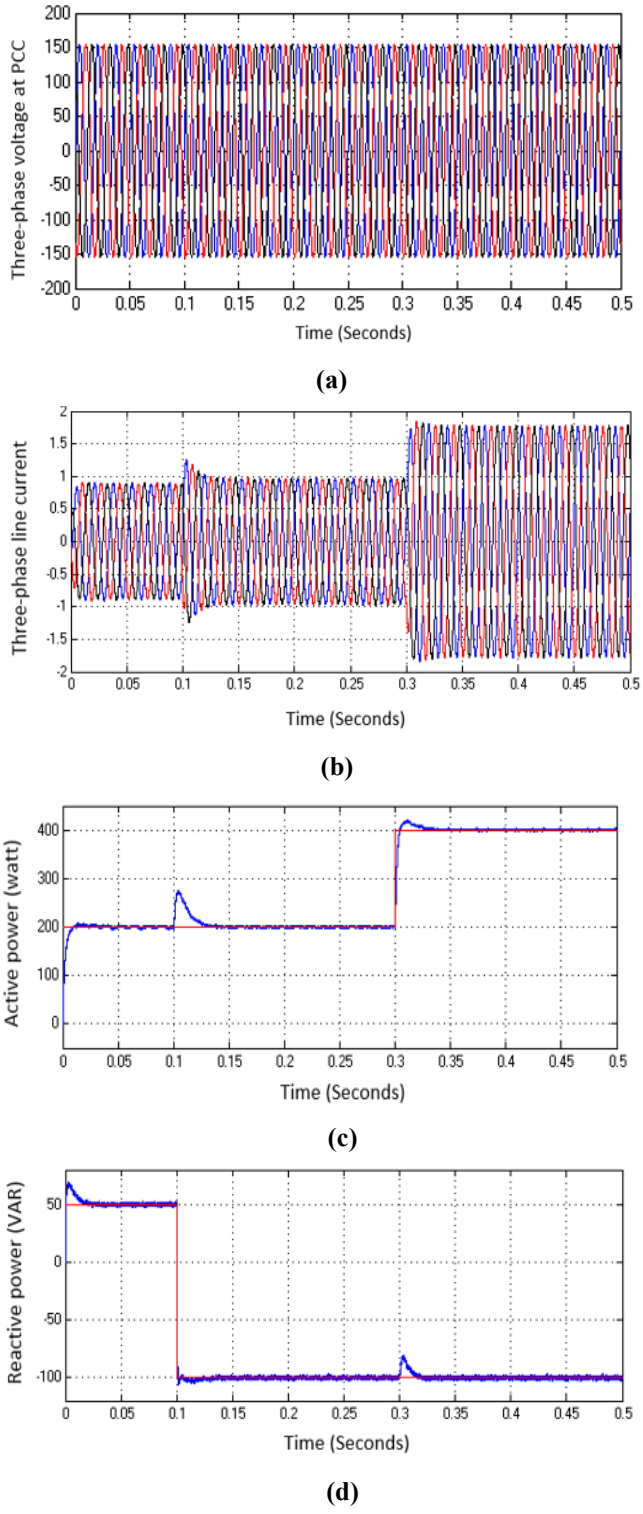

Fig.4 *Active and reactive power tracking by PI controller*

power reference are shown in the solid line and the dark thick line shows the tracking power generated from distributed generation. The results show that the active power and reactive power are tracked efficiently.

The reactive power reference is changed based on voltage variation. The purpose of changing the reactive power reference is to create a reactive power mismatch between inverter and the load. So, the reactive power mismatch shifts the frequency from its nominal value when islanding occurs. The new reactive power reference is set by using (14). The variation in frequency when Vpcc is less than $0.98*V_N$ is shown in Fig. 5 (a). Fig. 5 (b) represents the variation in frequency when Vpcc is greater than $1.01*V_N$

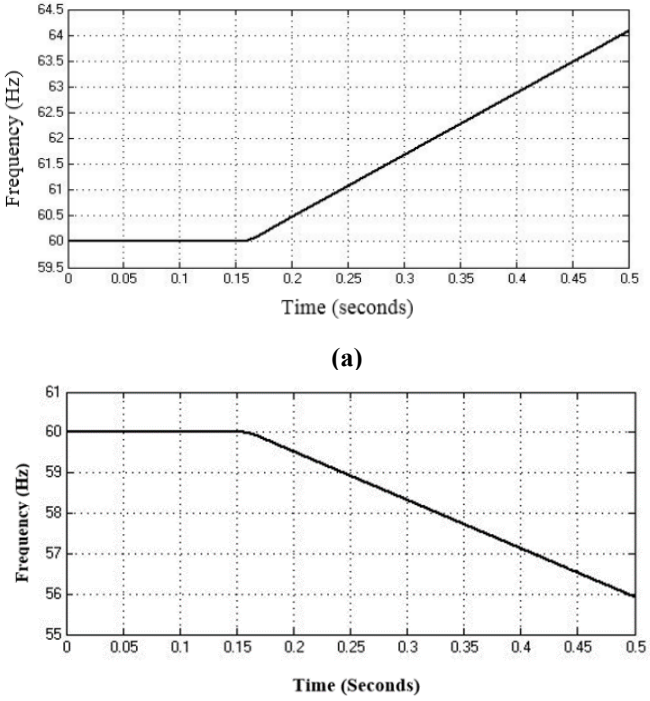

Fig. 5 *Frequency variation due to change in reactive power*

The proposed algorithm detects islanding condition in all kind of loads and has negligible non-detection zone. The results show that the variations in frequency due to islanding is very high as compared to the variation due to switching of capacitors or load. So, the proposed method can easily differentiate the islanding event with other disturbances in the system. Frequency variation is the key parameter in this technique to detect islanding. Simulation results show the efficiency of islanding detection method.

IV. Conclusion

In this paper, an islanding detection method is proposed based on frequency deviation. Adaptive reactive power mismatch is proposed to detect islanding event in weak grid and worst load conditions. By relaxing the frequency limits, the proposed method can differentiate the islanding event with other disturbances in the system (like sudden increase in load or capacitor switching). The result shows that the proposed adaptive reactive power mismatch helps in detecting islanding events. Moreover, the proposed method cannot affect the power quality of the electrical network. Implementing the proposed islanding detection method on multiple houses is yet to explore. We will include it in future work.

Acknowledgment

The authors acknowledge the support of Macquarie University through the International Research Training Program.

References

[1] P. Gupta, R. S. Bhatia, and D. K. Jain, "Average Absolute Frequency Deviation Value Based Active Islanding Detection Technique," *IEEE Trans. Smart Grid*, vol. 6, no. 1, pp. 26–35, Jan. 2015, doi: 10.1109/TSG.2014.2337751.

[2] B. Ahmadzadeh-Shooshtari, M. E. H. Golshan, and A. Rezaei-Zare, "Fast and systematic approach for adjusting ROCOF relay used in islanding detection of SDG," *IET Gener. Transm. Distrib.*, vol. 14, no. 2, pp. 275–283, Jan. 2020, doi: 10.1049/iet-gtd.2019.0352.

[3] M. Malakondaiah, K. K. Boddeti, B. R. Naidu, and P. Bajpai, "Second harmonic impedance drift-based islanding detection method," *IET Gener. Transm. Distrib.*, vol. 13, no. 23, pp. 5313–5324, Dec. 2019, doi: 10.1049/iet-gtd.2018.6838.

[4] C. R. Aguiar, G. Fuzato, R. F. Bastos, A. F. Q. Gonçalves, and R. Q. Machado, "Hybrid fuzzy anti-islanding for grid-connected and islanding operation in distributed generation systems," *IET Power Electron.*, vol. 9, no. 3, pp. 512–518, Mar. 2016, doi: 10.1049/iet-pel.2014.0717.

[5] A. Kazemi and H. Pourbabak, "Islanding detection method based on a new approach to voltage phase angle of constant power inverters," *IET Gener. Transm. Distrib.*, vol. 10, no. 5, pp. 1190–1198, Apr. 2016, doi: 10.1049/iet-gtd.2015.0776.

[6] G. Marchesan, M. R. Muraro, G. Cardoso, L. Mariotto, and A. P. de Morais, "Passive Method for Distributed-Generation Island Detection Based on Oscillation Frequency," *IEEE Trans. Power Deliv.*, vol. 31, no. 1, pp. 138–146, Feb. 2016, doi: 10.1109/TPWRD.2015.2438251.

[7] P. K. Ganivada and P. Jena, "Passive Islanding Detection Techniques Using Synchrophasors for Inverter Based Distributed Generators," in *2019 IEEE PES GTD Grand International Conference and Exposition Asia, GTD Asia 2019*, May 2019, pp. 747–751, doi: 10.1109/GTDAsia.2019.8715902.

[8] Y. M. Makwana and B. R. Bhalja, "Islanding detection technique based on superimposed components of voltage," *IET Renew. Power Gener.*, vol. 11, no. 11, pp. 1371–1381, Sep. 2017, doi: 10.1049/iet-rpg.2016.0942.

[9] D. U. Kim and S. Kim, "Anti-islanding detection method using phase shifted feed-forward voltage," in *Conference Proceedings - IEEE Applied Power Electronics Conference and Exposition - APEC*, May 2019, vol. 2019-March, pp. 1480–1486, doi: 10.1109/APEC.2019.8721890.

[10] A. Yafaoui, B. Wu, and S. Kouro, "Improved Active Frequency Drift Anti-islanding Detection Method for Grid Connected Photovoltaic Systems," *IEEE Trans. Power Electron.*, vol. 27, no. 5, pp. 2367–2375, May 2012, doi: 10.1109/TPEL.2011.2171997.

[11] B. Wen, D. Boroyevich, R. Burgos, Z. Shen, and P. Mattavelli, "Impedance-Based Analysis of Active Frequency Drift Islanding Detection for Grid-Tied Inverter System," *IEEE Trans. Ind. Appl.*, vol. 52, no. 1, pp. 332–341, Jan. 2016, doi: 10.1109/TIA.2015.2480847.

[12] H. Vahedi and M. Karrari, "Adaptive Fuzzy Sandia

Frequency-Shift Method for Islanding Protection of Inverter-Based Distributed Generation," *IEEE Trans. Power Deliv.*, vol. 28, no. 1, pp. 84–92, Jan. 2013, doi: 10.1109/TPWRD.2012.2219628.

[13] J. Tao, H. Han, Z. Wang, Y. Shu, W. Fang, and Y. Li, "An Advanced Islanding Detection Strategy Coordinating the Newly Proposed v Detection and the ROCOF Detection," in *International Conference on Innovative Smart Grid Technologies, ISGT Asia 2018*, Sep. 2018, pp. 1204–1208, doi: 10.1109/ISGT-Asia.2018.8467902.

[14] S. Akhlaghi, A. A. Ghadimi, and A. Akhlaghi, "A novel hybrid islanding detection method combination of SMS and Q-f for islanding detection of inverter- based DG," in *2014 Power and Energy Conference at Illinois (PECI)*, Feb. 2014, pp. 1–8, doi: 10.1109/PECI.2014.6804571.

[15] S. Akhlaghi, A. Akhlaghi, and A. A. Ghadimi, "Performance analysis of the Slip mode frequency shift islanding detection method under different inverter interface control strategies," in *2016 IEEE Power and Energy Conference at Illinois (PECI)*, Feb. 2016, pp. 1–7, doi: 10.1109/PECI.2016.7459250.

[16] S. Liu, S. Zhuang, Q. Xu, and J. Xiao, "Improved voltage shift islanding detection method for multi-inverter grid-connected photovoltaic systems," *IET Gener. Transm. Distrib.*, vol. 10, no. 13, pp. 3163–3169, Oct. 2016, doi: 10.1049/iet-gtd.2015.1151.

[17] R. Zamani and M. E. H. Golshan, "Islanding detection of synchronous machine-based distributed generators using signal trajectory pattern recognition," in *Proceedings - 2018 6th International Istanbul Smart Grids and Cities Congress and Fair, ICSG 2018*, Jul. 2018, pp. 91–95, doi: 10.1109/SGCF.2018.8408949.

[18] H. Laaksonen and P. Hovila, "Islanding Detection during Intended Island Operation of Nested Microgrid," in *Proceedings - 2018 IEEE PES Innovative Smart Grid Technologies Conference Europe, ISGT-Europe 2018*, Dec. 2018, doi: 10.1109/ISGTEurope.2018.8571571.

[19] R. Azim, F. Li, Y. Xue, M. Starke, and H. Wang, "An islanding detection methodology combining decision trees and Sandia frequency shift for inverter-based distributed generations," *IET Gener. Transm. Distrib.*, vol. 11, no. 16, pp. 4104–4113, Nov. 2017, doi: 10.1049/iet-gtd.2016.1617.

[20] Dong Dong, Bo Wen, P. Mattavelli, D. Boroyevich, and Yaosuo Xue, "Modeling and Design of Islanding Detection Using Phase-Locked Loops in Three-Phase Grid-Interface Power Converters," *IEEE J. Emerg. Sel. Top. Power Electron.*, vol. 2, no. 4, pp. 1032–1040, Dec. 2014, doi: 10.1109/JESTPE.2014.2345783.

[21] D. Dong, D. Boroyevich, P. Mattavelli, B. Wen, and Y. Xue, "Anti-islanding protection in three-phase converters using grid synchronization small-signal stability," in *2012 IEEE Energy Conversion Congress and Exposition (ECCE)*, Sep. 2012, pp. 2712–2718, doi: 10.1109/ECCE.2012.6342385.

[22] W. Zahoor and S. H. Zaidi, "Synchronization and dq current control of grid-connected voltage source inverter," in *17th IEEE International Multi Topic Conference 2014*, Dec. 2014, pp. 462–466, doi: 10.1109/INMIC.2014.7097384.

[23] S. Raza, H. Mokhlis, H. Arof, J. A. Laghari, and H. Mohamad, "A Sensitivity Analysis of Different Power System Parameters on Islanding Detection," *IEEE Trans. Sustain. Energy*, vol. 7, no. 2, pp. 461–470, Apr. 2016, doi: 10.1109/TSTE.2015.2499781.